Astron. & Astrophys. 29, 1–6 (1973)

Line Profiles and Turbulence Generated by Acoustic Waves in the Solar Chromosphere

I. Absorption Profiles and Height Variation of Velocity Amplitudes

L. Oster

Joint Institute for Laboratory Astrophysics* and Department of Physics and Astrophysics, University of Colorado, Boulder

P. Ulmschneider

Astronomisches Institut der Universität Würzburg, Germany

Received February 29, 1972, revised May 6, 1973

Summary. Line profiles produced by Doppler effects due to acoustic waves with velocity profiles ranging from purely sinusoidal to sawtooth-type shock waves are computed in the temperature range typical for the solar chromosphere. The results can be used as local absorption profiles in the computation of the profiles of emerging chromospheric lines. The height variation of velocity profiles and amplitudes is deduced from previous model calculations by Ulmschneider.

Key words: acoustic waves – line profiles – microturbulence – solar chromosphere

1. Introduction

Reliable values of microturbulent velocities v_t are among the most urgently needed basic parameters in computations of stellar atmospheres. So far, these values have been determined observationally with the source of the associated gas motion treated as unknown. Moreover even the solar observations of the microturbulent velocities v_t were, up to very recent times, poorly determined. At the Bilderberg Conference on the Solar Atmosphere, for example, the participants could not arrive at a definite conclusion as to even the sign of the height derivative dv_t/dh. In most computations of stellar atmospheres v_t represents simply an empirical constant to give the best fit to the observed line profiles.

Thus it appears highly desirable to look for a theoretical basis for the computation of microturbulent velocities. One possible source of the chromospheric microturbulence are acoustic waves which are produced in the convection zone and balance the radiative losses in the chromosphere and corona.

It is the purpose of this paper to lay the groundwork for a detailed investigation of this problem. We discuss in Section 2 the velocity profiles of the oscillations, and compute in Section 3 the resulting absorption profiles. In Section 4 we propose a model run of profiles with height which can be used to determine the profiles of emergent chromospheric lines.

* Operated jointly by the National Bureau of Standards and the University of Colorado.

2. Velocity Profiles

The velocity profiles which we investigate develop out of monochromatic sound waves and thus exhibit all intermediate stages of development between a purely

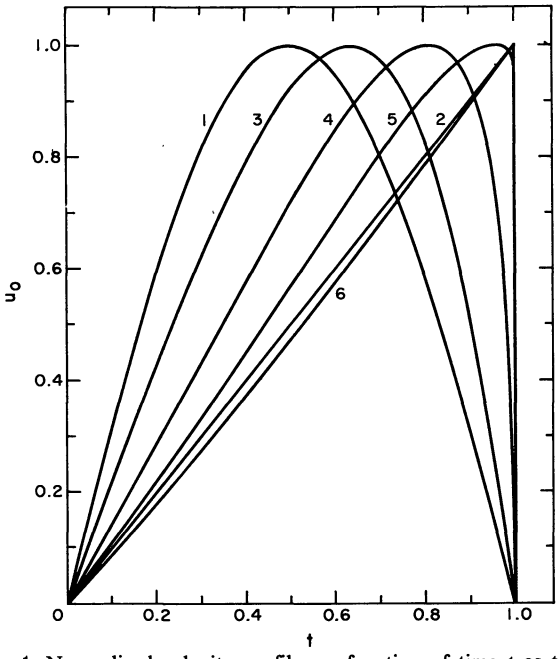

Fig. 1. Normalized velocity profiles as function of time t as taken from Ulmschneider (1971). One half period is shown. Case 1 indicates a purely sinusoidal profile, case 2 a linear sawtooth shock. Profiles 3 to 5 represent intermediate cases, while profile 6 corresponds to a so-called exponential shock

sinusoidal wave and a sawtooth shock wave. The common characteristic of such waves is that they are periodic consisting of monotonically rising and continuously falling parts. As we consider waves with small amplitudes, the temporal velocity profiles at a certain space point are such that the negative velocities are mirror images of the positive profiles. Hence, to represent one whole period of the wave it suffices to show only the half period where the velocity is positive. In Fig. 1 we have plotted a series of wave profiles which were computed by Ulmschneider (1971). Since we shall in general not need the actual magnitude of the velocity amplitude, it suffices to list here the normalized velocity profiles. The magnitudes were also given by Ulmschneider (1971) who computed them on the basis of acoustic wave spectra, called EE and SE spectra (Stein, 1968), which were sliced into a series of monochromatic waves propagating on top of the Harvard Smithsonian Reference Atmosphere (Gingerich *et al.*, 1971). We can assume that the velocity values on which we base our computation are fairly representative of what one expects from wave amplitudes and profiles in the outer solar atmosphere. This statement becomes the more valid the lower the heights are in the atmosphere. At any rate, the range of normalized profiles covers the spectrum of currently contemplated wave forms.

3. The Absorption Profiles

If the region of a stellar atmosphere, where a spectral line is formed, is permeated by periodic waves with velocity amplitudes between the extreme values of $-u_0$ and $+u_0$, a particular element will produce a spectral line which is Doppler shifted by amounts that vary between $+\lambda_0 u_0/c$ and $-\lambda_0 u_0/c$, λ_0 being the rest wavelength of the line, c the speed of light. If furthermore the width of the line-forming region in the atmosphere is greater than the wavelength of the periodic disturbance, or if the time over which measurements are integrated is greater than the period of the oscillation, then the observed line profile will represent a weighted average over all Doppler shifts between the above given limits.

We are primarily concerned with periodic waves in which the velocity rises monotonically from a negative to a positive maximum and falls thereafter monotonically back to the negative maximum. The number of gas elements, dn, causing a Doppler shift $\lambda_0 u/c$ is proprotional to the time, dt, for which the elements are at velocity u with respect to the observer, that is,

$$dn = \text{const} \cdot dt = \text{const} \left(\left[\frac{du}{dt}\right]_r^{-1} + \left[\frac{du}{dt}\right]_f^{-1} \right) du . \tag{1}$$

Here r labels the rising, f the falling part of the velocity profile. The constant, inverse of the wave period, is determined by the normalization condition

$$\int dn = \text{const} \cdot \int_{-u_0}^{+u_0} \left(\left[\frac{du}{dt}\right]_r^{-1} + \left[\frac{du}{dt}\right]_f^{-1} \right) du = 1 . \tag{2}$$

In the case of a discontinuity, no contribution originates in the falling portion of the profile.

Since we will be mostly concerned with the center of spectral lines, that is, the Doppler core, we describe the contour of the unshifted line by a gaussian profile, viz.,

$$I d\lambda = \frac{I_0}{\sqrt{\pi}\Delta\lambda_D} e^{-\alpha^2} d\lambda , \tag{3}$$

where the intensity is normalized so that

$$\int I d\lambda = I_0 . \tag{4}$$

The Doppler width $\Delta\lambda_D$ is given as usual by

$$\Delta\lambda_D^2 = \frac{2kT}{m_0} \frac{\lambda_0^2}{c^2} , \tag{5}$$

and the (whole) half-width of the line reads

$$\Delta\lambda_{1/2} = 2(\ln 2)^{1/2} \Delta\lambda_D . \tag{6}$$

Here, the temperature T refers to the line emitting element whose mass is m_0; c and k, respectively, are the speed of light and Boltzmann's constant; λ_0 is the rest wavelength of the spectral line as before. The variable α in Eq. (3), finally, is defined by

$$\alpha = \frac{\lambda - \lambda_0}{\Delta\lambda_D} . \tag{7}$$

a) Sound Waves

If the waves are true sound waves, we can describe them by harmonic oscillations so that (Fig. 1, case 1)

$$u = u_0 \sin(2\pi\nu t) , \tag{8}$$

where ν is the frequency of the oscillation. Writing K for the normalization constant, we have from Eq. (1) the expression

$$dn = K(1 - u^2/u_0^2)^{-1/2} \frac{du}{2\pi\nu u_0} , \tag{9}$$

and with the aid of the normalization condition (2)

$$dn = (1 - u^2/u_0^2)^{-1/2} \frac{du}{\pi u_0} . \tag{10}$$

This leads to a normalized line profile

$$\varphi_1(\lambda) d\lambda = \begin{cases} \left[1 - \dfrac{(\Delta\lambda)^2}{(\Delta\lambda_S)^2}\right]^{-1/2} \dfrac{d\lambda}{\pi\Delta\lambda_S} , \\ \qquad\qquad \text{for} \quad |\lambda - \lambda_0| \leqq \Delta\lambda_S , \\ 0 , \quad \text{elsewhere} , \end{cases} \tag{11}$$

where

$$\Delta\lambda_S = \frac{u_0}{c} \lambda_0 . \tag{12}$$

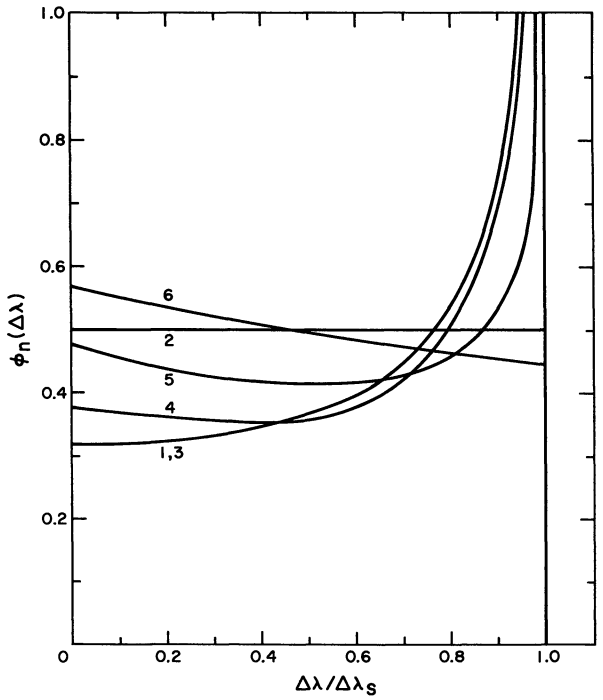

Fig. 2. Normalized line profiles $\varphi_n(\Delta\lambda)$ produced by the velocity oscillations of the waves of Fig. 1. $\varphi_n(\Delta\lambda)$ is plotted versus $\Delta\lambda/\Delta\lambda_S$ for the velocity profiles 1 to 6 from Fig. 1

The normalized profile φ_1 is shown in Fig. 2, case 1. Folding this profile into the gaussian of Eq. (3) we obtain

$$I_1 d\lambda = \frac{I_0 d\lambda}{\sqrt{\pi}\Delta\lambda_D}\,\frac{1}{\pi u_0} \int_{-u_0}^{+u_0} \exp[-(\lambda(1-u/c)-\lambda_0)^2/(\Delta\lambda_D)^2]\,\frac{du}{(1-u^2/u_0^2)^{1/2}}\,. \tag{13}$$

Introducing the quantity

$$\beta = \frac{\Delta\lambda_S}{\Delta\lambda_D} \tag{14}$$

and recalling that

$$\frac{\Delta\lambda_D}{\lambda} \approx \frac{\Delta\lambda_D}{\lambda_0} \ll 1\,, \tag{15}$$

we find

$$I d\lambda = \frac{I_0}{\Delta\lambda_D} d\lambda \frac{1}{\pi^{3/2}} \int_{-1}^{+1} e^{-(\alpha-\beta y)^2}(1-y^2)^{-1/2}\,dy\,. \tag{16}$$

We have computed the normalized line contour

$$\varphi_1(\lambda)d\lambda = \frac{1}{\pi^{3/2}} \int_{-1}^{+1} \cdot \exp[-(\alpha-\beta y)^2]\,(1-y^2)^{-1/2}\,dy\,\frac{d\lambda}{\Delta\lambda_D} \tag{17}$$

for parameter values of β between 0 (gaussian profile) and 2.5 and plotted them in Fig. 3.

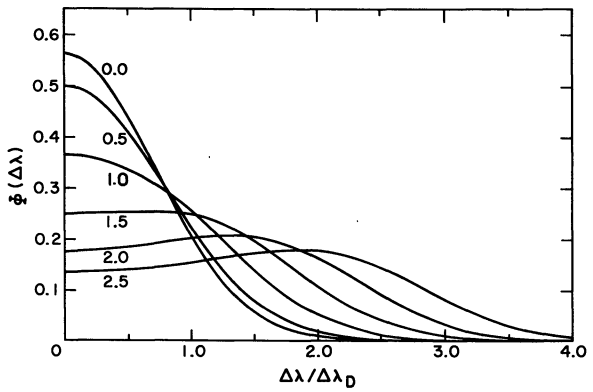

Fig. 3. Normalized line profiles $\varphi(\Delta\lambda)$ of *sinusoidal* waves (cases 1, 3, and 4 of Figs. 1 and 2) folded into a gaussian profile as function of $\alpha = \Delta\lambda/\Delta\lambda_D$. The curves are labeled by $\beta = \Delta\lambda_S/\Delta\lambda_D$

We shall comment on some specific features of this case at the end of this Section.

b) Shock Waves

For fully developed shock waves the case of linear "sawtooth" shocks may be treated analytically. This velocity profile is given by the expression

$$u = u_0 vt \tag{18}$$

and shown in Fig. 1, case 2. Thus we have

$$dn = K\frac{du}{u_0 v} \tag{19}$$

with

$$K = \frac{1}{2}v\,. \tag{20}$$

This leads to the normalized profile for linear sawtooth shocks (Fig. 2, case 2)

$$\varphi_2(\lambda)d\lambda = \begin{cases} \frac{1}{2}\,\frac{d\lambda}{\Delta\lambda_S}, & \text{for } |\lambda-\lambda_0| \leqq \Delta\lambda_S\,, \\ 0\,, & \text{elsewhere}\,. \end{cases} \tag{21}$$

Folding this profile into the gaussian and recalling inequality (15), we obtain for the normalized line contour

$$\varphi_2(\lambda)d\lambda = \frac{2}{\sqrt{\pi}} \int_{-1}^{+1} e^{-(\alpha-\beta y)^2} dy\,\frac{d\lambda}{\Delta\lambda_D}\,. \tag{22}$$

The integral can be expressed in terms of the error function (Abramowitz and Stegun, 1964; p. 297)

$$\Phi_2(\lambda)d\lambda = \frac{2}{\sqrt{\pi}\beta} \int_{\alpha-\beta}^{\alpha+\beta} e^{-z^2} dz\,\frac{d\lambda}{\Delta\lambda_D} = \frac{1}{\beta}\Big(\mathrm{erf}(\alpha+\beta)-\mathrm{erf}(\alpha-\beta)\Big)\frac{d\lambda}{\Delta\lambda_D}\,. \tag{23}$$

Figure 4 shows $\Phi_2(\lambda)$ for an appropriate range of parameters β.

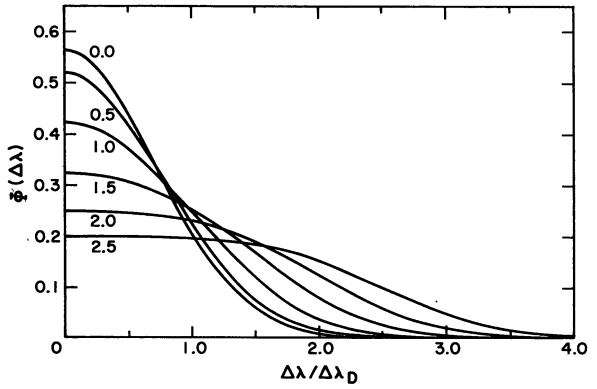

Fig. 4. Normalized line profiles $\Phi(\Delta\lambda)$ of *sawtooth* waves (case 2 of Figs. 1 and 2) folded into a gaussian profile as function of $\alpha=\Delta\lambda/\Delta\lambda_D$. The curves are labeled by $\beta=\Delta\lambda_S/\Delta\lambda_D$

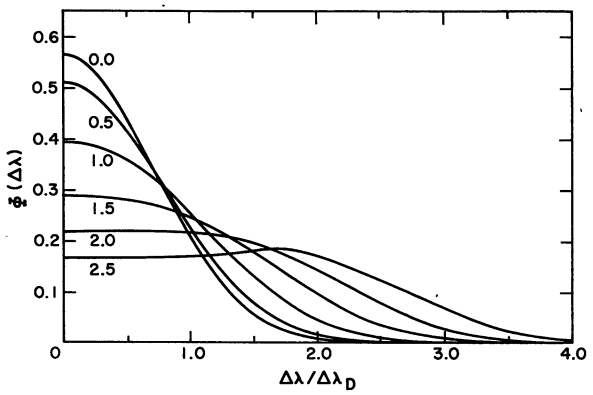

Fig. 5. Normalized line profiles $\Phi(\Delta\lambda)$ of the *intermediate* shock wave (case 5 of Figs. 1 and 2) folded into a gaussian profile as function of $\alpha=\Delta\lambda/\Delta\lambda_D$. The curves are labeled by $\beta=\Delta\lambda_S/\Delta\lambda_D$

c) Intermediate Cases

For intermediate cases where we have a distorted sinusoidal wave profile (Fig. 1, cases 3, 4, and 5) and for a case where we have an "exponential-type sawtooth shock" (Fig. 1, case 6) the normalized profiles shown in Fig. 2, cases 3–6, may be computed with the aid of Eq. (1) by numerical means:

$$\varphi_n(\lambda)d\lambda=\begin{cases} K_nF_n\left(\dfrac{\Delta\lambda}{\Delta\lambda_S}\right)\dfrac{d\lambda}{\Delta\lambda_S}, & \text{for } |\lambda-\lambda_0|\leqq\Delta\lambda_S, \\ 0, & \text{elsewhere.} \end{cases} \quad (24)$$

The constants K_n are determined by the normalization condition of Eq. (2). The folded line contour is then obtained from the expression

$$\Phi_n(\lambda)d\lambda=\frac{K_n}{\sqrt{\pi}}\int_{-1}^{+1}\exp[-(\alpha-\beta y)^2]F_n(y)dy\frac{d\lambda}{\Delta\lambda_D}. \quad (25)$$

The actual computations were carried out using a 64-point Gaussian integration scheme and are represented in Figs. 3–5 as follows:

Profile 3 was found to have practically the same normalized profile as a pure sound wave and thus in turn led to the folded profile of the pure sound wave. However, it was surprising that profile 4 which is considerably distorted by comparison with pure sinusoidal shape still resulted in a folded profile that again was for all practical purposes identical with the folded sinusoidal profile.

Profile 5 with its large discontinuity is a more typical intermediate case. The folded profile of this case is shown in Fig. 5. The folded profile 6, finally departs only by a few percent from a linear sawtooth profile and is therefore not graphed separately.

In concluding this discussion we would like to draw attention to the saddle shape of the contour φ_1 for essentially simusoidal waves, if β is in excess of unity. This shape is, of course, reminiscent of the innermost portions of the CaII-lines H and K in the solar and stellar spectra. However, in the case of the solar chromosphere, where the line centers are formed in regions permeated by shock waves rather than sinusoidal waves, the observed contour is not due to this profile reversal (Shine and Oster, 1973).

4. Wave Patterns and Turbulent Velocities in the Solar Chromosphere

Conventionally, the cores of spectral lines in stellar atmospheres are described by gaussian profiles whose half-width is expressed in terms of a thermal velocity, v, to which usually a so-called turbulent velocity, v_t, is added:

$$\Delta\lambda_D=(v^2+v_t^2)^{1/2}\lambda_0/c. \quad (26)$$

The thermal velocity v depends on the mass m of the element involved, so that

$$v^2=(m_H/m)v_0^2, \quad (27)$$

where

$$v_0^2=2kT/m_H, \quad (28)$$

and m_H is the mass of the hydrogen atom, while v_t is supposedly independent of m.

This type of analysis assumes that there is a gaussian distribution of Doppler shifts due to random motions of gas elements. We have seen that this is not the case, if the atmosphere is permeated by periodic waves, and the analysis of line profiles in terms of turbulent velocities in this case is only approximately correct.

Indeed, it is *a priori* not clear to what extent the contour of an emergent spectral line differs in the cases where, on one hand, we assume along the line of sight a gaussian distribution of random motions with a certain mean velocity, and, on the other hand, a periodic motion with the same velocity amplitude, folding either distribution into a thermal Doppler distribution to yield the complete profile of the absorption coefficient. This will

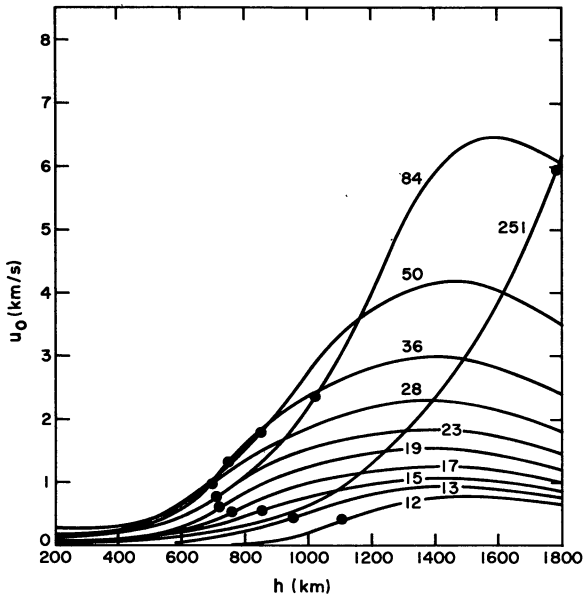

Fig. 6. Velocity amplitude u_0 as function of height h of monochromatic acoustic waves propagating on top of the Harvard-Smithsonian Reference Atmosphere as computed from data by Ulmschneider (1971). The EE *spectrum* was used. The dot to the left indicates the height below which the waves are sinusoidal, the dot to the right the height above which they are of the sawtooth type. The numbers label wave periods

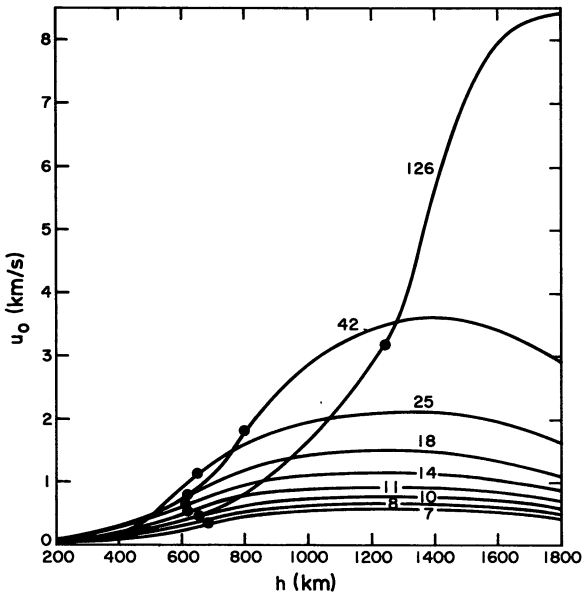

Fig. 7. Velocity amplitude u_0 as function of height h of monochromatic acoustic waves propagating on top of the Harvard Smithsonian Reference Atmosphere as computed from data by Ulmschneider (1971). The SE *spectrum* was used. The dot to the left indicates the height below which the waves are simusoidal, the dot to the right the height above which they are of the sawtooth type. The numbers label wave periods

be the subject of separate investigations (Shine and Oster, 1973).

In order to make a realistic comparison with observational data, we must further specify the height variation of both the wave velocities and of the wave profiles. For this purpose, we show in Figs. 6 and 7 the maximum amplitudes u_0 of the wave velocities as computed by Ulmschneider (1971), with the wave period as parameter. Dots separate low altitude regions, where sinusoidal profiles prevail, from high altitude regions where sawtooth profiles dominate. The change from an essentially sinusoidal to a fully developed sawtooth profile is accomplished in a height interval of about 150 km.

Inspection of Figs. 6 and 7 shows that Stein's SE and EE spectra produce quite similar velocity amplitudes. This similarity is in part due to the requirement that a certain amount of flux crosses the chromosphere at 800 km. Comparing the u_0-values shown in Figs. 6 and 7 with the thermal velocities deduced from the electron temperatures of the Harvard Smithsonian Reference Atmosphere, we see that all β-values are well below unity for hydrogen atoms. On the other hand, heavy elements such as Mg and Ca will correspond to much larger β-values, since β is proportional to $(m/m_H)^{1/2}$, m being the mass of the element in question, m_H the mass of the hydrogen atom.

Before we are able to apply these theoretical considerations to the problem of line formation in the solar chromosphere, we have to decide as to the u_0-values to

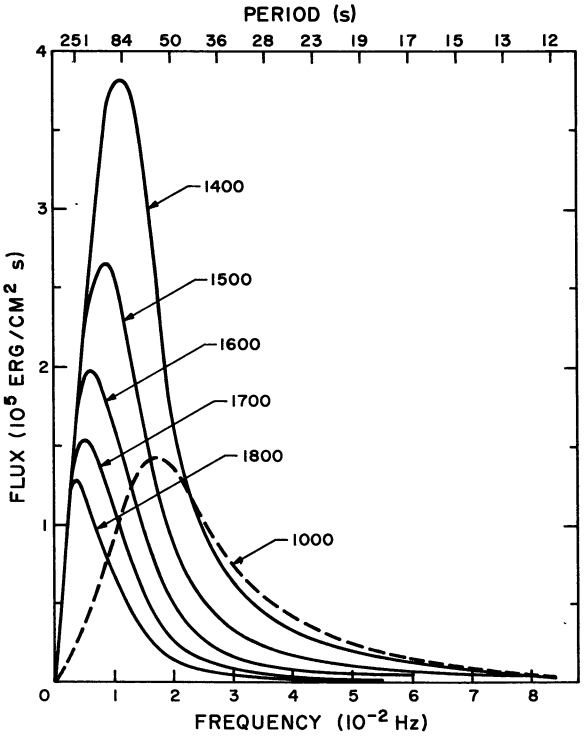

Fig. 8. Acoustic flux as function of frequency at various heights (in km) resulting from the propagation and dissipation of a series of monochromatic waves propagating on top of the Harvard-Smithsonian Reference Atmosphere and starting with the EE spectrum. The flux spectrum at 1000 km is scaled down by a factor of 10. The periods of the 11 members are indicated on the top scale

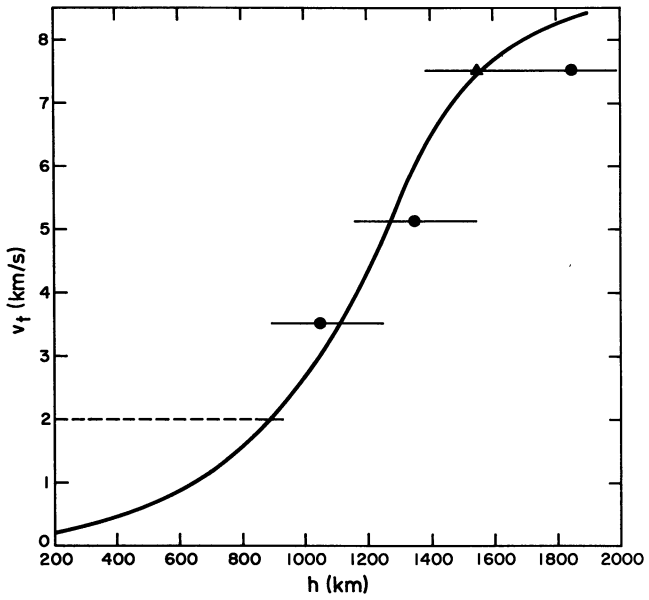

Fig. 9. Velocity amplitude u_0 as function of height h (solid line). Dots show observed microturbulent velocities given by Athay (1970) based on various sources for comparison. The triangle shows the O I line results. Horizontal bars indicate roughly the observational height uncertainty. At lower heights the observations of Canfield (1971) and other authors are shown by the dashed line

be associated with a given height in the chromosphere. At any given time waves of various periods are likely to be present and the local absorption profile will be an average over a range of profiles corresponding to different u_0's. However, we may expect that the flux model, i.e., the distribution of wave energy versus period, gives an indication of the frequency with which, in the average, a specific u_0 will occur at each height, and for a first orientation assign to each such chromospheric height level the u_0 value of the there dominant oscillation. It is shown in a subsequent paper (Shine and Oster, 1973) that the results of this simplified procedure do not differ significantly from one which is based on a whole spectrum of u_0 values.

As the first step in this program, we have plotted in Fig. 8 the monochromatic acoustic flux as a function of frequency for the height levels 1000 to 1800 km. The spectrum shifts towards lower frequencies at greater altitude because of the dissipation of shock waves of higher frequency. It is readily seen that at 1000 km the 50 s, at 1400 the 83 s, at 1600 the 100 s and at 1800 the 251 s waves predominate. The velocity amplitudes u_0 of these dominant oscillations may be taken from Figs. 6 and 7. Because u_0 is less than the thermal velocity v_0 for hydrogen, β is less than unity for hydrogen whereas for atoms of higher mass the β-values are mostly greater than one.

In order to see whether any effect worth initiating an extensive computational program is to be expected, we have plotted in Fig. 9 (solid line) u_0 as a function of height in the Harvard-Smithsonian Reference Atmosphere under the assumption that the actual velocity amplitude is indeed determined by the energetically dominant wave mode. For comparison we have entered (dots) microturbulent velocities observed from Mg b1, Na D, O I and the H + K lines of Ca II as given by Athay and Skumanich (1968), Athay and Canfield (1969), Athay (1970), Canfield (1971). The height values given by Athay (1970) were increased by 340 km to change the zero height level from the limb to $\tau_{5000} = 1$. The triangle indicates the height where the O I lines with $v_t = 7$–8 km/s are thought to originate (Athay, 1961, 1970; Jones and Rense, 1970). The horizontal bars in Fig. 9 indicate uncertainties in height measurements.

It is now immediately obvious that our u_0-values follow rather closely the run of observed turbulent velocities, except that some discrepancy is seen near the temperature minimum region where Canfield (1971), whose numbers are in good agreement with other determinations, reports residual turbulence with a velocity of the order of 2 km/s. Apparently the horizontal turbulent velocity is larger than the vertical velocity at these heights (Athay and Canfield, 1969). This type of turbulence may simply be due to a different mechanism, such as gravity waves.

In summary, we see that Ulmschneider's model of acoustic wave propagation leads to velocity amplitudes that are fairly close to observed turbulent velocities. In a subsequent paper these velocity amplitudes will be used together with the absorption profiles computed in Section 3 to calculate the emergent line profiles of the solar Ca II and Mg II K lines.

References

Abramowitz, M., Stegun, I.A. 1964, Handbook of Mathematical Functions. Nat. Bureau of Standards, Washington
Athay, R.G. 1961, *Astrophys. J.* **134**, 756
Athay, R.G. 1970, *Solar Phys.* **12**, 175
Athay, R.G., Canfield, R.C. 1969, *Astrophys. J.* **156**, 695
Athay, R.G., Skumanich, A. 1968, *Solar Phys.* **4**, 176
Canfield, R.C. 1971, *Solar Phys.* **20**, 275
Gingerich, O., Noyes, R.W., Kalkofen, W., Cuny, Y. 1971, *Solar Phys.* **18**, 347
Jones, R.A., Rense, W.A. 1970, *Solar Phys.* **15**, 317
Shine, R.A., Oster, L. 1973, *Astron. & Astrophys.* **29**, 7
Stein, R. 1968, *Astrophys. J.* **154**, 297
Ulmschneider, P. 1971, *Astron. & Astrophys.* **12**, 297

Ludwig Oster
Joint Institute for Laboratory Astrophysics
University of Colorado
Boulder, Colorado 80302, USA

Peter Ulmschneider
Astronomisches Institut der Universität
D-8700 Würzburg
Federal Republic of Germany